Supporting Information for:

INFLUENCE OF SUBSTRATES ON THE LONG-RANGE ORDER OF PHOTOELECTRODEPOSITED SE-TE NANOSTRUCTURES

ETHAN SIMONOFF[†], MICHAEL F. LICHTERMAN[†], KIMBERLY M. PAPADANTONAKIS[†], NATHAN S. LEWIS[†,‖,*]

[†]Division of Chemistry and Chemical Engineering. 127-72, 210 Noyes Laboratory

[‖]Beckman Institute

California Institute of Technology

Pasadena, CA 91125

*Corresponding Author: nslewis@caltech.edu

S1. Contents

S2. Experimental methods and materials

Chemicals and Materials SeO_2 (Aldrich, 99.999% trace metals basis), TeO_2 (Aldrich, 99.995% trace metals basis), Buffer HF Improved (BHF) (Transene, Ammonium Hydrogen Difluoride Solution), H_2SO_4 (J.T. Baker, 90-100%), Nickel Sulfamate Solution (Transene), Ga (Alfa Aesar, 6mm diameter pellets, 99.9999% trace metals basis), In (ESPI Metals, shot, 99.9999%), Acetone (BDH, ACS Grade, 99.5% min.), Isopropyl Alcohol (BDH, ACS Grade, 99.5% min.), Ir wire (Alfa Products, 1mm dia., 99.9%), and Ni pellets (Kurt J. Lesker, ¼" dia. x ¼" long, 99.995%) were used as received. H_2O (Barnstead Nanopure Infinity Ultrapure Water System, ρ = 18.3 MΩ-cm) was used throughout.

Silicon substrates used as working electrodes include n^+ silicon (Addison Engineering Inc., As-doped, ρ = 0.001-0.004 Ω-cm, [111], 525 ± 25 μm thick, SSP) and p^+ silicon (Virginia Semiconductor Inc., B-doped, $\rho < 0.0025$ Ω-cm, [111], 500 ± 25 μm thick, SSP).

Loctite 1C Hysol Epoxy Adhesive, Conductive Silver Paint (SPI Supplies), Clear Nail Polish (Sally Hansen "Hard as Nails Xtreme Wear"), tinned Cu wire (AWG 22), and glass tubing (7740 Borosilicate Pyrex, 9mm OD x 1.0mm wall thickness) were used to fabricate electrodes.

Preparation of Au and Ti Metal Substrates Au and Ti substrates used as working electrodes in the deposition of Se-Te were fabricated via electron-beam evaporation of the target metals onto n^+-Si wafers. Prior to metal evaporation and loading into the vacuum chamber, n^+-Si wafers were etched in BHF until the native silicon oxide layer was removed from both the top and bottom sides of the Si. For Au substrates, 20 nm of Ti and 70 nm of Au were evaporated onto the polished side of n^+-Si; for Ti substrates, 100 nm of Ti was evaporated. Evaporated Ti was used as an ohmic contact layer to the n^+-Si (and additionally as an adhesion layer in the case of the Au

substrates). 20 nm of Ti was evaporated onto the back side of the n^+-Si wafers as an ohmic back contact for both substrates.

Silicon and Metal Electrode Fabrication Au substrates, Ti substrates, p^+-Si, and n^+-Si wafers were cleaved into small chips (between 0.01 cm^2 and 0.15 cm^2) to be fabricated into working electrodes. Ga-In eutectic (75.5 wt. % gallium, 24.5 wt. % indium) was prepared and scratched into the back of the n^+-Si and p^+-Si pieces using a carbide-tipped scribe. Electrode mounts were fabricated from glass tubing (~5-6 inches long) and tinned Cu wire bent into a flat coil and affixed to the glass tube using inert epoxy. The exposed flat coil on the electrode mount was placed in contact with the Ga-In coated surface of the silicon or metal-coated chip, and was glued in place using Ag paint. After the Ag paint had dried, clear nitrocellulose nail polish was applied to temporarily electrically insulate the tinned Cu wire, Ag paint, and backside of the electrode.

Iridium Wire Electrode Fabrication A piece of Ir wire (~30 mm) was soldered to a ~6 inch segment of tinned Cu wire and placed in a ~5 inch glass tube. The soldered contact and glass tube opening nearest to the Ir wire was insulated with inert epoxy.

Nickel Electrode Fabrication A single Ni pellet was soldered to a ~6 inch segment of tinned Cu wire. The soldered contact was insulated with inert epoxy.

Photoelectrochemical and Solid-State Measurements All electrochemical and solid-state measurements were performed using a Biologic VMP3 Potentiostat, controlled via EC Lab for Windows. The light intensity was measured using a calibrated Si photodiode (Thorlabs FDS100). A three-port Pyrex glass electrochemical cell with a flat glass window was utilized for all photoelectrochemical depositions and tests.

For electrochemical experiments, a three-electrode configuration was used with an Ir wire counter electrode and a Ag/AgCl (3M NaCl, BASi RE-5B) reference electrode. Working electrodes were p^+- or n^+- Si wafer pieces. Unless otherwise stated, most films were deposited until a charge density of -750 mC cm^{-2} had been passed. Depending on substrate and other parameters, various applied potentials were used in the deposition of Se-Te films (see Table S2). Silicon substrates were etched with BHF for ~20 s and rinsed with H_2O immediately before testing and deposition. The light source used in the deposition of most Se-Te films was a homemade LED apparatus fashioned out of an aluminum printed circuit board (PCB) (Sink Pad II 1939) fastened onto an Al block and cooled by chilled-water at a temperature of 14 °C. Thermal contact was obtained using an interfacial layer of Ag thermal paste (Arctic Silver 5 High-Density Polysynthetic Silver Thermal Compound). Three LEDs (Osram SFH 4725S) were soldered in series to the PCB. The LEDs had an intensity weighted average wavelength of 927 nm, a spectral bandwidth of 37 nm, and were powered by a DC power supply (Hewlett Packard E3611A) in constant current mode at 0.78 A. The output from the LEDs was passed through a dichroic film linear polarizer (Thorlabs LPNIRE200-B) and collected with an aspheric condenser lens (Edmund Optics, Ø = 75 mm, f = 50 mm). A 600 grit diffuser (Thorlabs DG20) was placed in front of the window of the electrochemical cell to produce illumination of uniform intensity incident on the working electrodes. An illumination power density of 53 mW cm^{-2} was used during the photoelectrochemical deposition.

For solid-state, ultraviolet photoemission spectroscopic (UPS), and x-ray photoemission spectroscopic (XPS) measurements, Se-Te films were grown for 10 min using unpolarized ~ 200 mW cm^{-2} illumination from a homemade broad-band white light source constructed from a 300 W ELH-type W-halogen bulb with an intensity weighted average wavelength of 640 nm at 120 V.

For solid-state measurements, top contact was made by electroplating Ni onto the deposited Se-Te films. For electrodeposited top contacts, Ni films were deposited from a Ni sulfamate solution in a three-electrode configuration with a Ni pellet counter electrode and a Ag/AgCl (1M KCl, CH Instruments, CHI111) reference electrode. Nickel films were deposited potentiostatically for ~2 h between -0.600 V and -0.800 V vs. Ag/AgCl, depending on the substrate. Nickel is known to make ohmic contact to both Se and Te[1, 2]. Contact was made to the deposited Ni film with a tinned Cu wire and Ag paint. To determine the current-voltage behavior of the Se-Te – Si junctions, a two-electrode configuration was utilized, with the Si substrate as the working electrode and the electrodeposited Ni top contact as the counter electrode.

Sample Preparation and Image Acquisition Following electrodeposition, a razor blade was utilized to cut samples from electrode mounts. Samples were then placed in an acetone bath to remove excess nail polish and Ag paint. All samples were imaged using an FEI Nova NanoSEM 450 with an accelerating voltage of 5 kV. A through-lens (immersion) secondary electron detector was utilized at a working distance of 5 mm. For Fourier analysis, samples were imaged at a magnification of 6250 X and resolution 4096 pixels wide, corresponding to a scale of ~85.8 pixels μm^{-1}. Gwyddion (http://gwyddion.net/) was used for all image analysis, Fourier Transform analysis and Lorentzian peak fitting. Horizontal and vertical surface profiles were extracted from 2D FT plots with an integration width of 30 pixels. Other images used were obtained at a magnification of 25k X and with a resolution 2048 pixels wide, corresponding to a scale of ~171.6 pixels μm^{-1}.

Work Function, Valence Band Position, and Compositional Analysis Work function, valence band position, and compositional analysis measurements were acquired using a Kratos AXIS Ultra XPS and UPS (Kratos Analytical, Manchester, UK). The x-ray source was the

monochromatic Al K α line at 1486.6 eV, with 0.2 eV resolution at full width half maximum. The ultraviolet source was a He I line at 21.22 eV photon energy. XPS and UPS data were analyzed using CasaXPS, CASA Software Ltd. Charge neutralization was not utilized during data acquisition. The XPS instrument was calibrated to the Au $4f_{7/2}$ peak at 84 eV. Samples were calibrated to the adventitious carbon peak at 284.5 eV. The UPS instrument was calibrated such that the zero binding-energy position was the Fermi edge of freshly sputtered Au.

To measure work functions, the linear portions of the secondary-electron cutoff in the UPS data were extrapolated to the x-intercept positions, as shown by the linear fit lines in Figure S3. The x-intercept values were then subtracted from the He I photon energy (21.22 eV) to yield the work function values for the Se-Te films.

For valence-band positions, the linear portions of the low binding-energy regions in the UPS data were extrapolated to the x-intercept positions, as shown by the linear fit lines in Figure S3. The x-intercept values were then added to the observed Fermi level/work function values to obtain the valence-band maxima (VBM).

S3. Low-magnification SEM images used for FT analysis in Figure 1.

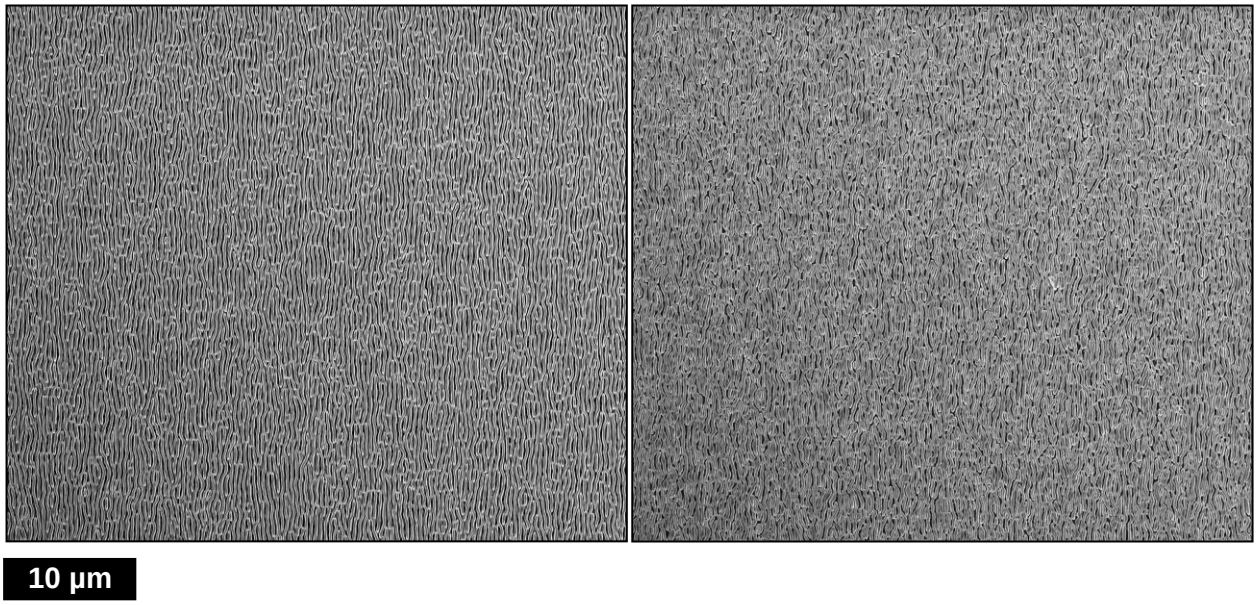

Figure S1. Low-magnification SEM images of photoelectrodeposited Se-Te films grown on (a) p^+-Si/Figure 1(a) and (b) n^+-Si/Figure 1(b) used in Fourier analysis in Figure 1(c)-(f). SEM images are obtained at a magnification of 6250X and at a resolution of 4096 pixels wide, corresponding to a scale of 85.8 pixels μm^{-1}.

S4. Additional data gathered for Se-Te films deposited on n^+-Si and p^+-Si substrates.

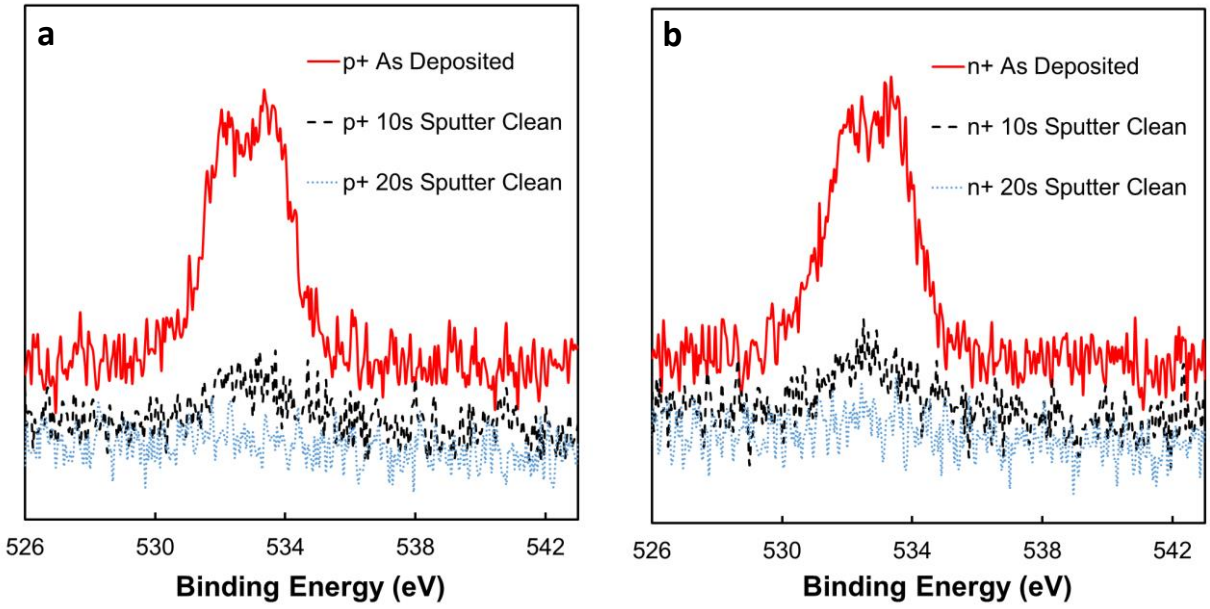

Figure S2. XPS data of O 1s (Se-O and Te-O) core-level region for as deposited; 10 s sputter cleaned; and 20 s sputter cleaned Se-Te films on (a) p^+-Si and (b) n^+-Si substrates, showing the progressive removal of a surface oxide after sputter cleaning.

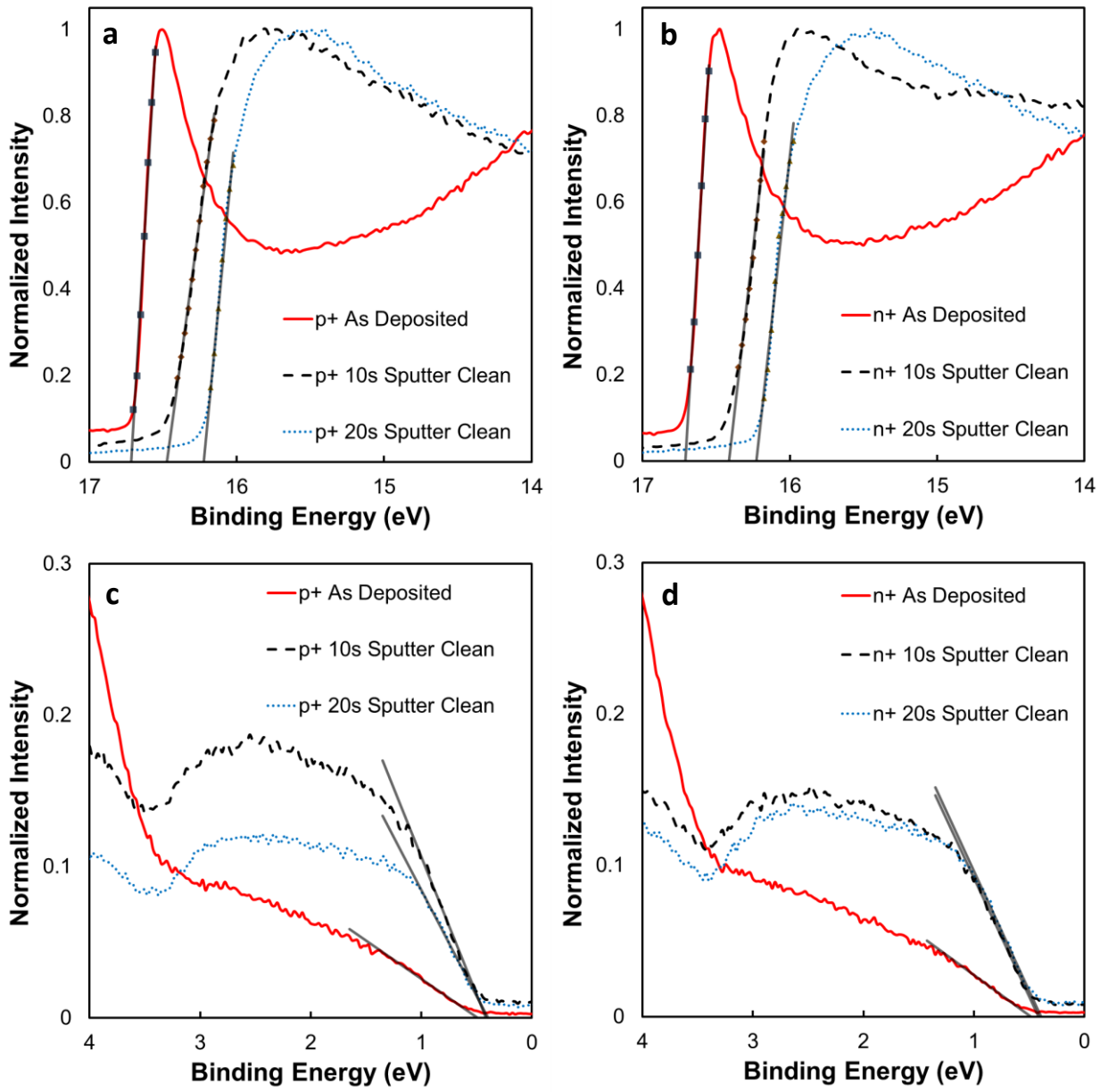

Figure S3. Normalized UPS data for as deposited, 10 s sputter cleaned, and 20 s sputter cleaned Se-Te films showing work function and valence band maximum positions on (a), (c) p^+-Si and (b), (d) n^+-Si substrates. The spectra show that the work function values shifted to a higher kinetic energy as the surface oxide on Se-Te was gradually removed by sputter cleaning.

Table S1. List of Work Function and Valence Band Maxima (VBM) Values Calculated from UPS Spectra

Sample	VBM - E_F (eV)	Work Function (eV)
n+ As Deposited	0.486 ± 0.017	4.51 ± 0.10
n+ 10s Sputter Cleaning	0.416 ± 0.014	4.81 ± 0.15
n+ 20s Sputter Cleaning	0.395 ± 0.015	4.99 ± 0.15
p+ As Deposited	0.488 ± 0.014	4.51 ± 0.09
p+ 10s Sputter Cleaning	0.415 ± 0.017	4.75 ± 0.20
p+ 20s Sputter Cleaning	0.396 ± 0.013	5.00 ± 0.12

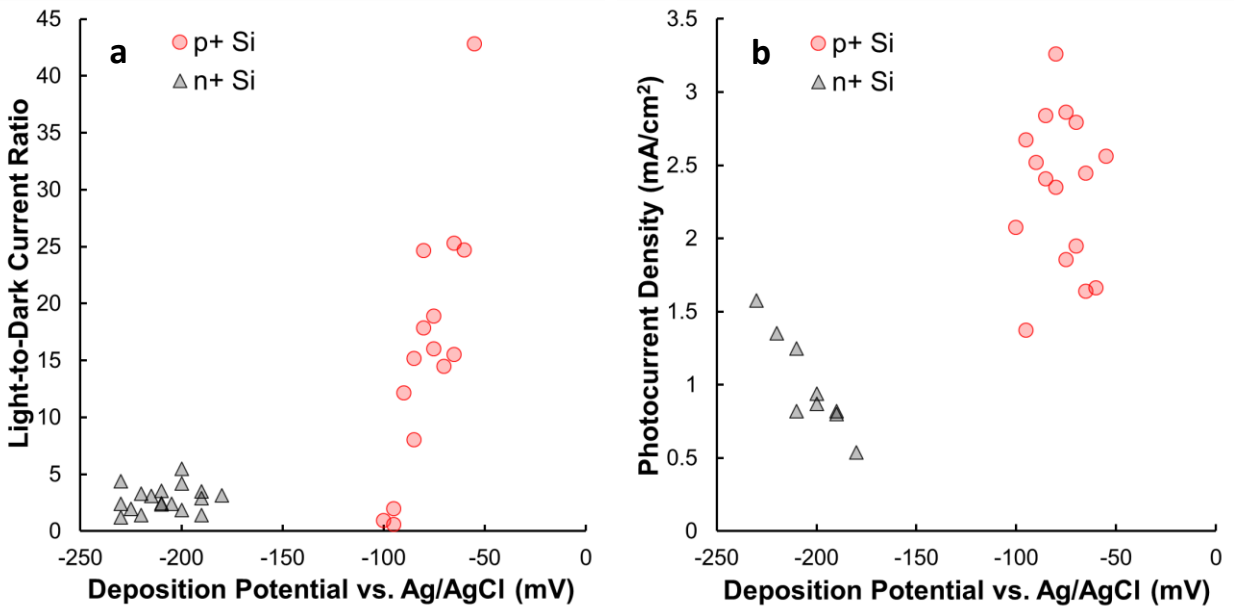

Figure S4. Plots showing the relationship between (a) light-to-dark current ratios (measured during chopped light chronoamperometry) and (b) measured peak photocurrent densities vs. the applied potential in the deposition of Se-Te on p^+-Si and n^+-Si. At peak current during growth, the light-to-dark current ratios sharply increased at more negative deposition potentials on p^+-Si, whereas on n^+-Si these ratios exhibited little to no trend with deposition potential. Peak photocurrent densities showed nearly no relationship to deposition potential for films deposited on p^+-Si. On n^+-Si, a stronger trend yielded a higher photocurrent density (and more extracted photocurrent) at more negative deposition potentials. The unchanging (with applied potential) light-to-dark current ratios on n^+-Si suggest that the photo- and dark-current densities increased concomitantly as films were deposited at more negative potentials. On p^+-Si, however, photocurrent densities were more stable to changes in applied potential, suggesting no change in extracted photocurrent but rather purely a change in dark current densities as the deposition potential was made more negative. The experiments shown here depict the range of working potentials for which the photoelectrodeposition produced lamellar structures (rather than purely

dark growth or no growth) on either substrate. A relatively more negative applied potential is required for phototropic growth to occur on n^+-Si vs. p^+-Si.

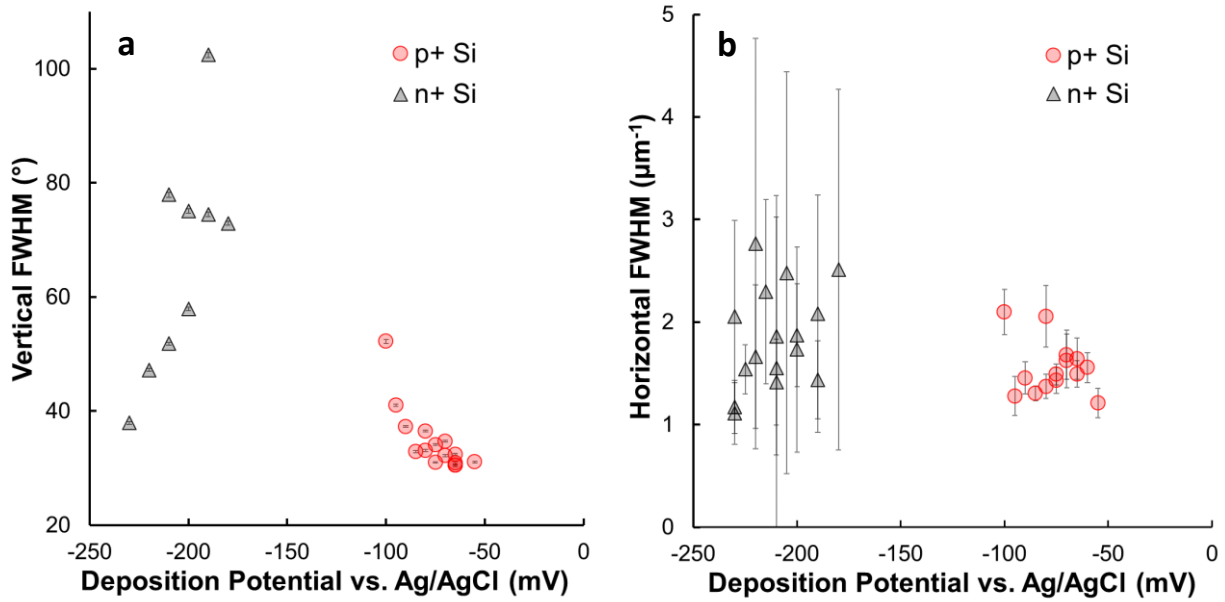

Figure S5. Plots showing the relationship between the (a) vertical and (b) horizontal primary peak FWHM in the FT spectra of SEM images of Se-Te films deposited on p^+-Si or n^+-Si vs. the potential applied in the deposition of those films. The horizontal FWHM did not track well with deposition potential, due to both a low signal-to-noise ratio and less pattern fidelity information encoded in the horizontal (perpendicular to input polarization) periodicity of the Se-Te film pattern. Conversely, in the vertical direction, the FWHM had a stronger relationship with deposition potential, with different trends observed for films grown on p^+-Si and n^+-Si. Straighter patterns were observed when deposition potentials were more positive on p^+-Si; however, on n^+-Si, straighter patterns developed with more negative relative applied potentials.

S5. Results and data gathered for Se-Te films deposited on Au and Ti substrates.

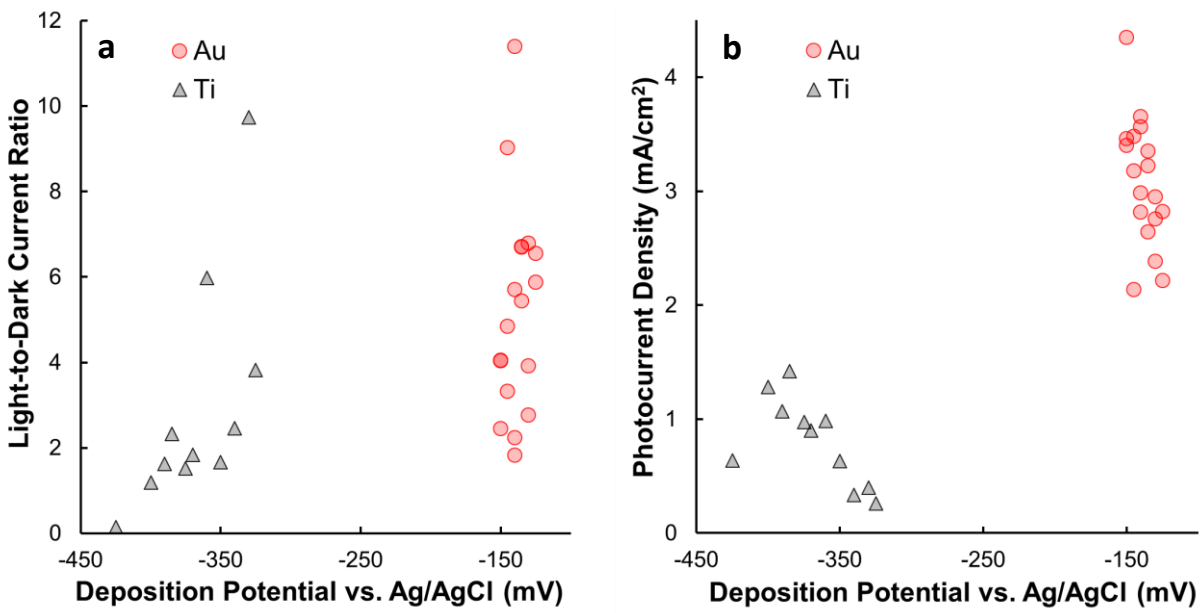

Figure S6. Plots showing the relationship between (a) light-to-dark current ratios (measured during chopped light chronoamperometry) and (b) measured peak photocurrent densities vs. the applied potential in the deposition of Se-Te on Au and Ti substrates. Se-Te films deposited on Au substrates generally displayed higher measured light-to-dark current ratios and higher photocurrent densities than were observed for films deposited on Ti substrates.

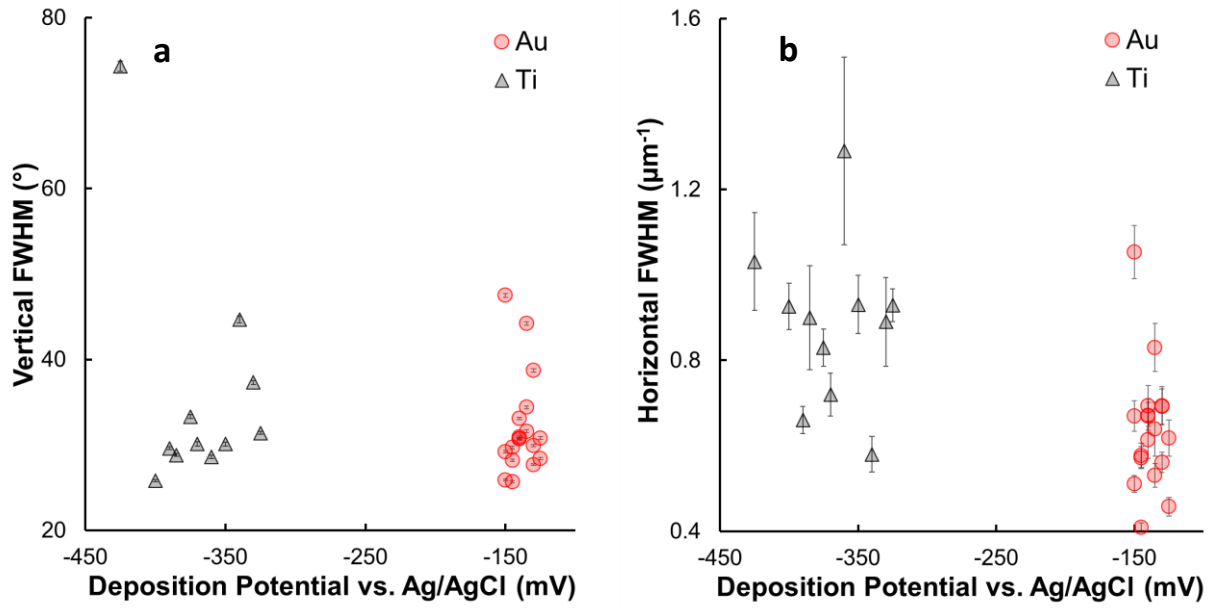

Figure S7. Plots showing the relationship between the (a) vertical and (b) horizontal primary peak FWHM in the FT spectra of SEM images of Se-Te films deposited on Au or Ti substrates vs. the potential applied in the deposition of those films. Similar to the results on Si substrates, the horizontal FWHM data was noisier and provided less information on the pattern fidelity of Se-Te films relative to the observed vertical FWHM values. In general, straighter and higher fidelity patterns were observed in Se-Te films deposited on Au vs. Ti substrates.

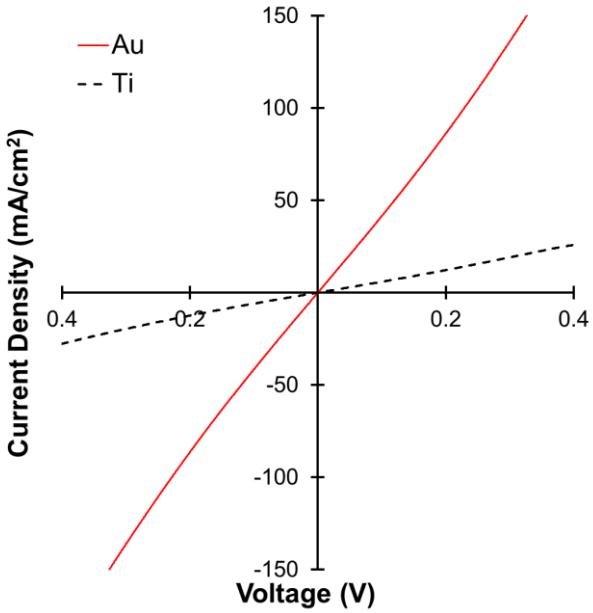

Figure S8. Current-voltage behavior of Se-Te on Au and Ti. As expected, better electrical contact and lower contact resistance was observed between Se-Te and Au, due to the closer work function alignment of Se-Te to Au relative to Ti.

S6. Low-magnification SEM images of Se-Te films on p^+-Si in Figure 5.

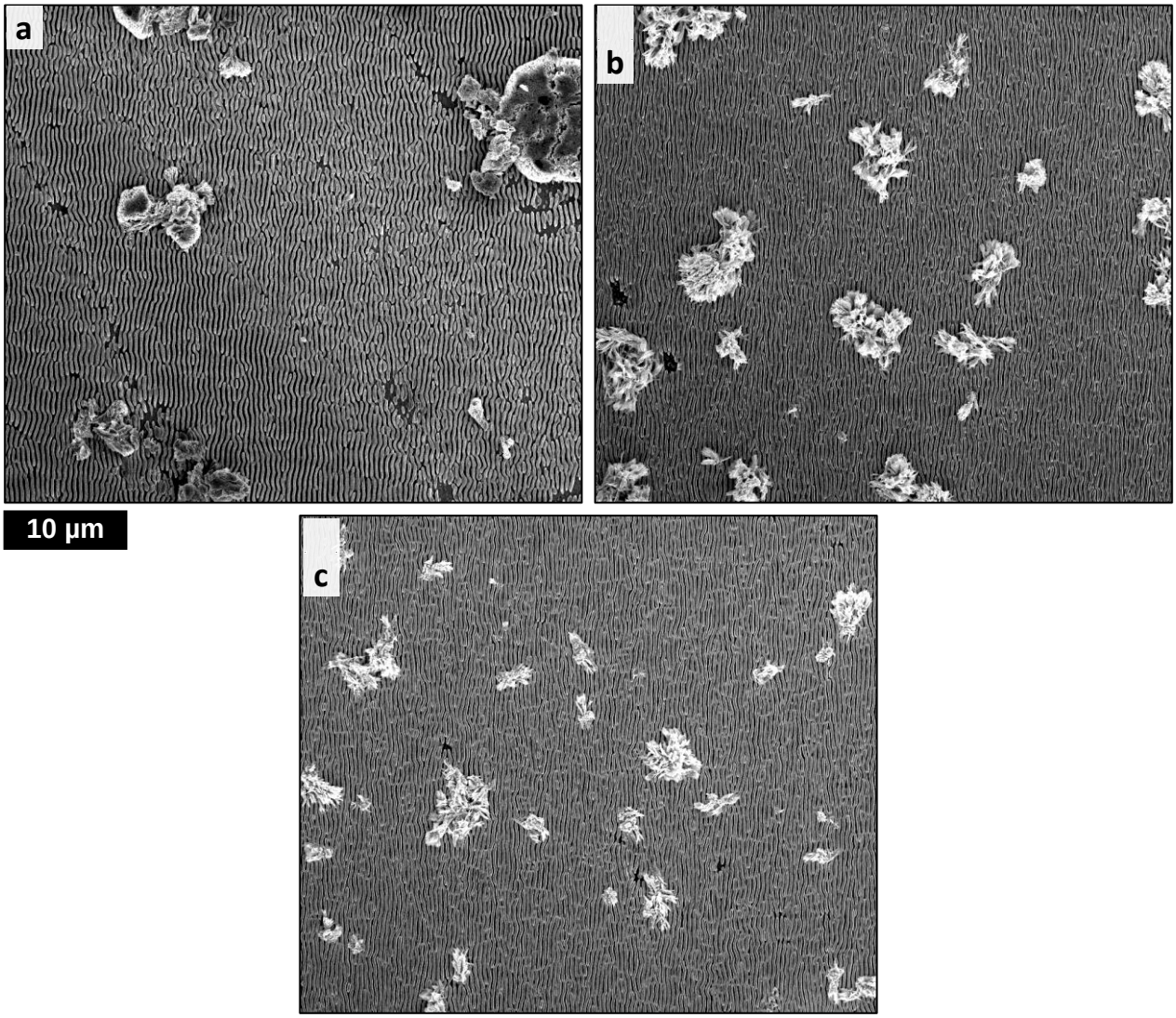

Figure S9. Low-magnification SEM images of photoelectrodeposited Se-Te films grown on p^+-Si from (a) Figure 5(a), (b) Figure 5(c), and (c) Figure 5(e), showing dark spherulitic/dendritic growth. The dark growth appearing on these films was unavoidable at the dark current densities and more negative applied potentials necessary to match the dark deposition rates on n^+-Si in Figure 5(b), (d), and (f).

S7. Nucleation density and growth substrate discussions.

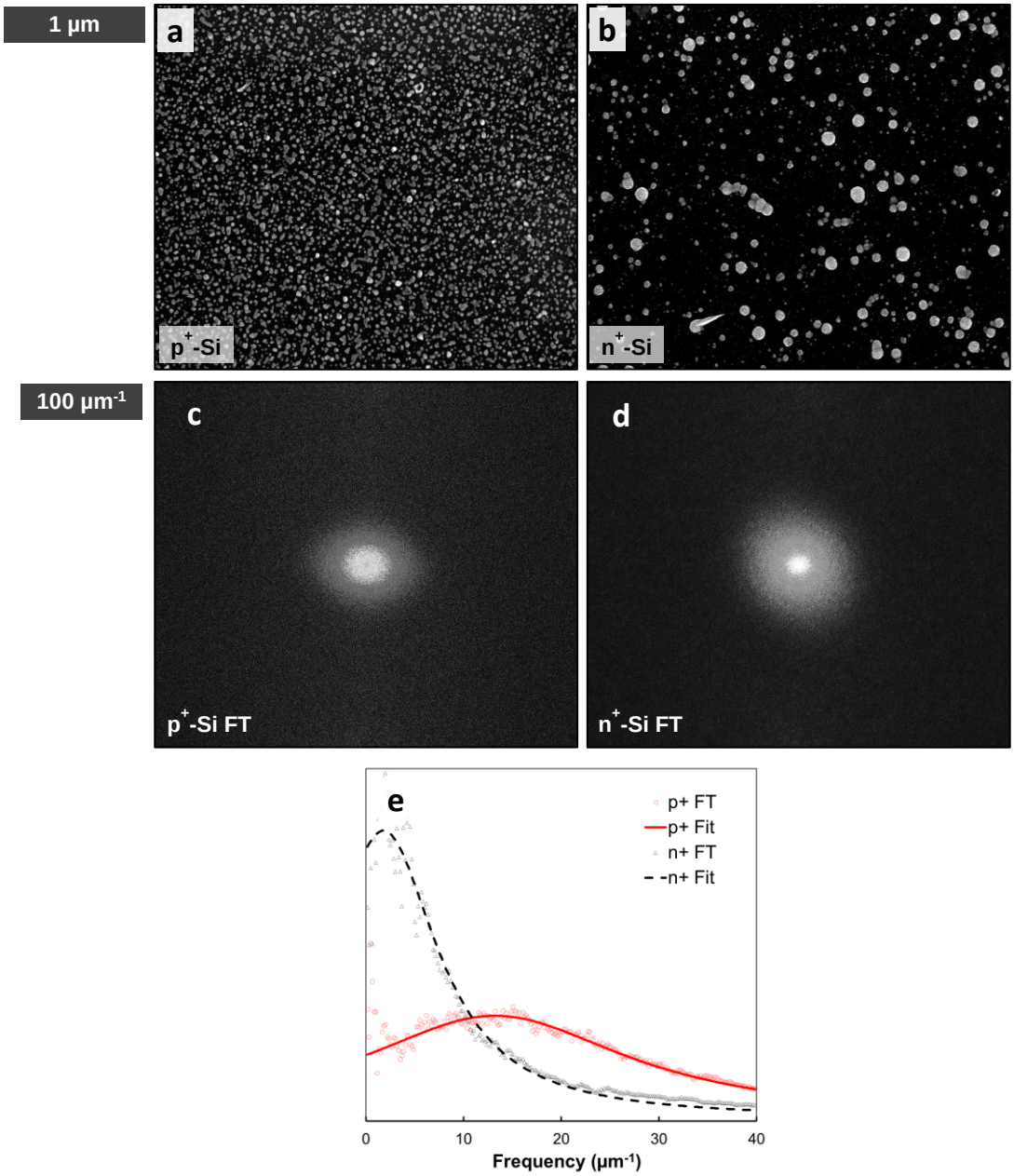

Figure S10. Nucleated Se-Te films deposited on (a) p^+-Si and (b) n^+-Si at a charge passed of -3.75 mC cm^{-2}. 2D FT of the images on (c) p^+-Si and (d) n^+-Si in (a) and (b), respectively. (e) Comparison of surface profile plots integrated radially over the FT spectra showing larger average particle-to-particle spacing for n^+-Si vs. p^+-Si. Isotropic peak shapes at this early level of deposition indicate random nucleation on both substrates. Although random, the peak positions in (e) are at

$13.2 \pm 0.05\ \mu m^{-1}$ and $1.8 \pm 0.07\ \mu m^{-1}$ for p^+-Si and n^+-Si, respectively, confirming the higher nucleation density observed on p^+-Si vs. n^+-Si. Random nucleation of Se-Te is hypothesized to be a required morphological precursor to the optical scattering effect that produces lamellar features in the photoelectrodeposit.[3-7] The morphology of phototropically grown Se-Te alloys is similar on a variety of substrates, as shown by past work primarily on either n^+-Si or Au. However, certain effects, such nucleation density, depend in detail quantitatively on the characteristics of the substrate, as seen in the variation between (a) and (b). The nucleation behavior also has implications for the pattern period and fidelity, implying quantitative differences between the phototropic film growth morphology on chemically different substrates as well as on substrates that only have mutually different electronic properties, such as doping density, as demonstrated herein.

S8. Table with additional information for all samples fabricated.

Table S2. List of Photoelectrochemical Details for All Samples Fabricated.

Figure ID	Sample ID	Substrate	Applied Potential (mV vs. Ag/AgCl)	Horizontal FWHM (μm^{-1})	Vertical FWHM (°)	Vertical FWHM (μm^{-1})	Peak Current Density (mA cm^{-2})	Light-to-Dark Current Ratio	Charge Passed (mC cm^{-2})	Illumination Power (mW cm^{-2})	Deposition Time (s)
F1, F3, S1, S4,	*138-4*	p^+	-65	1.49 ± 0.13	30.9 ± 0.16	1.51 ± 0.008	2.54	25.30	750	53	-
F1, F2, F3, S1, S4, S5	*140-9*	n^+	-200	1.77 ± 1.00	57.9 ± 0.31	2.74 ± 0.015	2.36	4.03	750	53	-
F2	*143-3*	p^+	-65	-	-	-	-	-	0.75	53	-
F2, S10	*143-2*	p^+	-65	-	-	-	-	-	3.75	53	-
F2	*143-4*	p^+	-65	-	-	-	-	-	37.5	53	-
F2	*143-5*	p^+	-65	-	-	-	-	-	75	53	-
F2, S4, S5	*142-10*	p^+	-65	1.06 ± 0.08	30.5 ± 0.16	1.52 ± 0.008	1.54	24.62	750	53	-
F2	*140-6*	n^+	-200	-	-	-	-	-	0.75	53	-
F2, S10	*140-7*	n^+	-200	-	-	-	-	-	3.75	53	-
F2	*144-1*	n^+	-200	-	-	-	-	-	37.5	53	-
F2	*144-2*	n^+	-200	-	-	-	-	-	75	53	-
F3	-	p^+	-200	-	-	-	-	-	-	200 (ELH)	600
F3	-	n^+	-200	-	-	-	-	-	-	200 (ELH)	600
F5, S9	*148-5*	p^+	-90	0.59 ± 0.03	33.7 ± 0.17	1.42 ± 0.007	0.52	2.22	750	16.56	-
F5, S9	*148-9*	p^+	-94	1.10 ± 0.07	30.1 ± 0.15	1.44 ± 0.007	0.69	2.74	750	14.91	-
F5, S9	*142-3*	p^+	-85	1.00 ± 0.08	31.4 ± 0.18	1.53 ± 0.009	1.03	3.91	750	20.88	-
F5, S4, S5	*137-8*	n^+	-205	2.48 ± 1.96	104.2 ± 0.57	5.86 ± 0.032	0.52	2.41	750	53	-
F5, S4, S5	*139-6*	n^+	-180	2.51 ± 1.76	72.9 ± 0.35	3.53 ± 0.017	0.71	3.17	750	53	-
F5, S4, S5	*139-1*	n^+	-200	1.73 ± 1.00	57.3 ± 0.30	2.54 ± 0.013	1.08	4.21	750	53	-
S4, S5	*136-3*	p^+	-100	2.10 ± 0.22	52.2 ± 0.34	3.10 ± 0.020	4.33	0.92	750	53	-
S4, S5	*136-4*	p^+	-75	1.49 ± 0.10	31.0 ± 0.13	1.71 ± 0.007	1.97	15.98	750	53	-

Figure ID	Sample ID	Substrate	Applied Potential (mV vs. Ag/AgCl)	Horizontal FWHM (μm^{-1})	Vertical FWHM (°)	Vertical FWHM (μm^{-1})	Peak Current Density (mA cm^{-2})	Light-to-Dark Current Ratio	Charge Passed (mC cm^{-2})	Illumination Power (mW cm^{-2})	Deposition Time (s)
S4, S5	*136-5*	p^+	-85	1.30 ± 0.07	32.9 ± 0.17	1.82 ± 0.009	2.57	15.15	750	53	-
S4, S5	*136-6*	p^+	-95	1.28 ± 0.19	41.0 ± 0.21	2.49 ± 0.013	3.83	0.56	750	53	-
S4, S5	*136-7*	p^+	-65	1.64 ± 0.20	32.4 ± 0.14	1.78 ± 0.008	1.74	15.52	750	53	-
S4, S5	*136-8*	p^+	-70	1.62 ± 0.26	34.7 ± 0.16	1.91 ± 0.009	2.08	14.46	750	53	-
S4, S5	*136-9*	p^+	-80	1.37 ± 0.12	33.1 ± 0.17	1.87 ± 0.010	2.48	17.86	750	53	-
S4, S5	*136-10*	p^+	-90	1.45 ± 0.16	37.3 ± 0.19	2.09 ± 0.011	2.73	12.14	750	53	-
S4, S5	*138-2*	p^+	-75	1.43 ± 0.13	34.1 ± 0.15	1.72 ± 0.008	3.01	18.88	750	53	-
S4	*138-5*	p^+	-85	-	-	-	3.19	7.99	750	53	-
S4, S5	*138-6*	p^+	-70	1.68 ± 0.24	32.2 ± 0.17	1.67 ± 0.009	2.83	77.47	750	53	-
S4, S5	*138-7*	p^+	-80	2.06 ± 0.30	36.5 ± 0.18	2.03 ± 0.010	3.39	24.64	750	53	-
S4, S5	*138-8*	p^+	-60	1.56 ± 0.15	30.5 ± 0.14	1.55 ± 0.007	1.73	24.69	750	53	-
S4	*138-9*	p^+	-95	-	-	-	4.05	1.94	750	53	-
S4, S5	*138-10*	p^+	-55	1.21 ± 0.14	31.1 ± 0.15	1.82 ± 0.009	2.62	42.79	750	53	-
S4	*137-1*	n^+	-200	-	-	5.66 ± 0.030	0.82	5.47	750	53	-
S4	*137-2*	n^+	-190	-	-	-	0.70	3.52	750	53	-
S4, S5	*137-3*	n^+	-210	1.55 ± 1.68	83.5 ± 0.44	4.53 ± 0.024	0.88	3.57	750	53	-
S4, S5	*137-4*	n^+	-220	2.76 ± 2.00	114.8 ± 0.64	5.70 ± 0.032	0.97	3.30	750	53	-
S4, S5	*137-5*	n^+	-230	2.05 ± 0.94	62.9 ± 0.37	3.19 ± 0.019	1.81	1.20	750	53	-
S4, S5	*137-6*	n^+	-230	1.11 ± 0.30	60.9 ± 0.27	2.81 ± 0.013	0.94	4.39	750	53	-
S4, S5	*137-7*	n^+	-215	2.30 ± 0.90	104.9 ± 0.49	5.61 ± 0.026	0.48	3.10	750	53	-
S4, S5	*137-10*	n^+	-225	1.54 ± 0.24	57.2 ± 0.30	2.82 ± 0.015	1.16	1.96	750	53	-
S4, S5	*139-2*	n^+	-190	1.44 ± 0.38	74.5 ± 0.40	3.50 ± 0.019	1.40	1.40	750	53	-
S4, S5	*139-3*	n^+	-210	1.41 ± 0.42	77.9 ± 0.42	3.29 ± 0.018	1.15	2.46	750	53	-

Figure ID	Sample ID	Substrate	Applied Potential (mV vs. Ag/AgCl)	Horizontal FWHM (μm^{-1})	Vertical FWHM (°)	Vertical FWHM (μm^{-1})	Peak Current Density (mA cm^{-2})	Light-to-Dark Current Ratio	Charge Passed (mC cm^{-2})	Illumination Power (mW cm^{-2})	Deposition Time (s)
S4, S5	*139-4*	n^+	-220	1.66 ± 0.70	47.2 ± 0.23	2.18 ± 0.011	2.30	1.42	750	53	-
S4, S5	*139-5*	n^+	-230	1.17 ± 0.26	37.9 ± 0.20	1.70 ± 0.009	2.24	2.39	750	53	-
S4, S5	*139-8*	n^+	-210	1.86 ± 1.16	51.8 ± 0.23	2.46 ± 0.011	1.78	2.34	750	53	-
S4, S5	*139-9*	n^+	-190	2.08 ± 1.16	102.4 ± 0.48	5.15 ± 0.024	1.08	2.90	750	53	-
S4, S5	*139-10*	n^+	-200	1.87 ± 0.50	75.1 ± 0.40	3.64 ± 0.019	1.45	1.85	750	53	-
S2, S3, Table S1	*82-1*	p^+	-200	-	-	-	-	-	-	200 (ELH)	600
S2, S3, Table S1	*82-4*	n^+	-200	-	-	-	-	-	-	200 (ELH)	600
S6, S7	*160-6*	Au	-135	0.64 ± 0.06	34.4 ± 0.16	1.53 ± 0.007	2.64	5.43	750	53	-
S6, S7	*160-7*	Au	-130	0.56 ± 0.02	27.7 ± 0.13	1.24 ± 0.006	2.38	2.76	750	53	-
S6, S7	*160-8*	Au	-150	0.67 ± 0.04	29.2 ± 0.14	1.30 ± 0.006	3.46	4.03	750	53	-
S6, S7	*161-1*	Ti	-350	0.93 ± 0.07	30.1 ± 0.25	1.60 ± 0.013	1.01	1.67	750	53	-
S6, S7	*161-2*	Ti	-375	0.83 ± 0.04	33.3 ± 0.24	1.78 ± 0.013	1.62	1.51	750	53	-
S6, S7	*161-3*	Ti	-400	0.93 ± 0.05	25.8 ± 0.13	1.42 ± 0.007	2.36	1.19	750	53	-
S6, S7	*161-4*	Ti	-425	1.03 ± 0.11	74.3 ± 0.59	4.57 ± 0.036	4.91	0.15	750	53	-
S6, S7	*161-5*	Ti	-325	0.93 ± 0.04	31.4 ± 0.16	1.67 ± 0.008	0.33	3.82	750	53	-
S6, S7	*161-6*	Au	-145	0.57 ± 0.03	28.2 ± 0.11	1.23 ± 0.005	3.18	4.84	750	53	-
S6, S7	*161-7*	Au	-140	0.67 ± 0.03	30.9 ± 0.16	1.39 ± 0.007	3.57	5.71	750	53	-
S6, S7	*161-8*	Au	-135	0.83 ± 0.06	44.2 ± 0.22	2.01 ± 0.010	3.22	6.69	750	53	-
S6, S7	*161-9*	Au	-130	0.69 ± 0.04	38.7 ± 0.20	1.72 ± 0.009	2.75	6.78	750	53	-
S6, S7	*161-10*	Au	-125	0.46 ± 0.02	30.8 ± 0.15	1.36 ± 0.007	2.21	6.55	750	53	-
S6, S7	*159-1*	Au	-150	1.05 ± 0.06	47.5 ± 0.24	2.12 ± 0.011	3.40	4.04	750	53	-
S6, S7	*159-2*	Au	-145	0.41 ± 0.01	25.7 ± 0.12	1.10 ± 0.005	2.14	9.02	750	53	-
S6, S7	*159-3*	Au	-140	0.61 ± 0.04	33.1 ± 0.15	1.42 ± 0.007	2.82	11.39	750	53	-

Figure ID	Sample ID	Substrate	Applied Potential (mV vs. Ag/AgCl)	Horizontal FWHM (μm^{-1})	Vertical FWHM (°)	Vertical FWHM (μm^{-1})	Peak Current Density (mA cm^{-2})	Light-to-Dark Current Ratio	Charge Passed (mC cm^{-2})	Illumination Power (mW cm^{-2})	Deposition Time (s)
S6, S7	*162-1*	Au	-150	0.51 ± 0.02	25.9 ± 0.12	1.15 ± 0.005	4.35	2.45	750	53	-
S6, S7	*162-2*	Au	-145	0.58 ± 0.03	29.7 ± 0.16	1.32 ± 0.007	3.48	3.32	750	53	-
S6, S7	*162-3*	Au	-140	0.69 ± 0.05	30.7 ± 0.14	1.38 ± 0.006	3.66	1.82	750	53	-
S6, S7	*162-4*	Au	-135	0.53 ± 0.03	31.6 ± 0.16	1.53 ± 0.008	3.35	6.71	750	53	-
S6, S7	*162-5*	Au	-130	0.69 ± 0.04	29.9 ± 0.15	1.34 ± 0.007	2.95	3.91	750	53	-
S6, S7	*162-6*	Au	-125	0.62 ± 0.04	28.4 ± 0.13	1.27 ± 0.006	2.82	5.87	750	53	-
S6, S7	*162-7*	Au	-140	0.67 ± 0.04	30.7 ± 0.15	1.38 ± 0.007	2.98	2.24	750	53	-
S6, S7	*163-2*	Ti	-360	1.29 ± 0.22	28.6 ± 0.19	1.39 ± 0.009	1.15	5.98	750	53	-
S6, S7	*163-3*	Ti	-385	0.90 ± 0.12	28.8 ± 0.16	1.53 ± 0.009	2.03	2.33	750	53	-
S6, S7	*163-6*	Ti	-330	0.89 ± 0.10	37.3 ± 0.22	1.74 ± 0.010	0.44	9.74	750	53	-
S6, S7	*163-8*	Ti	-340	0.58 ± 0.04	44.7 ± 0.40	2.24 ± 0.020	0.47	2.46	750	53	-
S6, S7	*163-9*	Ti	-370	0.72 ± 0.05	30.1 ± 0.25	1.59 ± 0.013	1.39	1.84	750	53	-
S6, S7	*163-10*	Ti	-390	0.66 ± 0.03	29.6 ± 0.16	1.55 ± 0.008	1.73	1.62	750	53	-

S9. References

1. Okuyama, K.; Tsuhako, J.; Kumagai, Y. *Thin Solid Films* **1975,** 30, 119-126.
2. Lanyon, H. P. D.; Krambeck, R. M., Trapping Levels in Hexagonal Selenium. In *The Physics of Selenium and Tellurium*, 1st ed.; Cooper, W. C., Ed. Pergamon Press: 1969; pp 59-68.
3. Sadtler, B.; Burgos, S. P.; Batara, N. A.; Beardslee, J. A.; Atwater, H. A.; Lewis, N. S. *Proc Natl Acad Sci U S A* **2013,** 110, 19707-12.
4. Carim, A. I.; Batara, N. A.; Premkumar, A.; Atwater, H. A.; Lewis, N. S. *Nano Lett* **2015,** 15, 7071-7076.
5. Carim, A. I.; Batara, N. A.; Premkumar, A.; Atwater, H. A.; Lewis, N. S. *ACS Nano* **2016,** 10, 102-11.
6. Carim, A. I.; Batara, N. A.; Premkumar, A.; May, R.; Atwater, H. A.; Lewis, N. S. *Nano Lett* **2016,** 16, 2963-8.
7. Carim, A. I.; Hamann, K. R.; Batara, N. A.; Thompson, J. R.; Atwater, H. A.; Lewis, N. S. *J Am Chem Soc* **2018,** 140, 6536-6539.